Contribution from the Department of Chemistry and Program in Molecular and Cellular Biology, University of Massachusetts, Amherst, Massachusetts 01003, Department of Chemistry, Institute of Materials Science, and Department of Chemical Engineering, University of Connecticut, Storrs, Connecticut 06269, and Department of Chemistry, University of California, Santa Cruz, California 95064

X-ray Spectroscopic Studies of Nickel Complexes, with Application to the Structure of Nickel Sites in Hydrogenases

Gerard J. Colpas,[†] Michael J. Maroney,*[,†,‡] Csaba Bagyinka,[†] Manoj Kumar,[†] William S. Willis,[§,∥] Steven L. Suib,[§,∥,⊥] Narayan Baidya,[#] and Pradip K. Mascharak[#]

Received July 3, 1990

X-ray absorption near-edge spectra (XANES) are reported for 44 Ni(II) and Ni(III) complexes with N- and/or S-donor ligands. The spectra reveal features associated with $1s \rightarrow 3d$ and $1s \rightarrow 4p_z$ electronic transitions, whose presence or absence and intensity provide information that allows the coordination number/geometry of the complex to be determined in most cases. The complexes in this study were selected in order to examine the reliability of coordination number/geometry assignments in complexes with low symmetry and to examine the effects on the spectra of a change in formal oxidation state from +II to +III. The effects on the spectra due to changes in the ligand environment are examined, and the edge energy and the breadth of the edge are found to correlate with the average hardness of the ligand environment. The effects on the spectra due to oxidation state changes are examined by using several pairs of Ni(II/III) isoleptic complexes. These compounds reveal that the effects of changes in the formal oxidation state of the Ni center are strongly dependent on the nature of the ligands present, with S-donor ligands giving rise to smaller shifts in edge energy than N,O-donor ligands. These trends are indicative of the increasing role of ligand oxidation in Ni(III) thiolate complexes. These trends are corroborated by X-ray photoelectron spectroscopic (XPS) studies that show a similar trend in both ligand and metal electron binding energies. The information obtained from the model studies is used to examine the Ni K-edge XANES spectrum obtained from a sample of *Thiocapsa roseopersicina* hydrogenase poised in form C. This spectrum is shown to be consistent with a distorted trigonal-bipyramidal geometry and a mixed O,N- and S-donor ligand environment for this biological Ni site.

Since the discovery of Ni as a component of the active site of the enzyme urease in 1975,[1] a total of four classes of enzymes have been identified that utilize Ni in specific ways. These classes include hydrogenase (H_2ase),[2,3] carbon monoxide dehydrogenase (CO dehydrogenase),[4] and methyl-S-coenzyme-M reductase,[5] in addition to urease.[6] A variety of physical studies have shown that Ni exists in distinct ligand environments in each of these enzymes. Urease contains a possibly dinuclear site,[7] consisting of six-coordinate Ni(II) centers bound to O,N-donor ligands derived from amino acids in the protein.[8] The Ni centers in urease are not known to be redox active and appear to play a role as Lewis acids in the hydrolysis of urea.[6] Three types of H_2ase exist, two of which contain redox-active Ni centers with S-donor ligands.[9,10] These two types of H_2ase Ni sites are distinguished by the presence or absence of a Se-donor ligand derived from a selenocysteine residue in the protein.[11,12] In many cases, a possible N-donor ligand has also been detected.[13] Sulfur ligation has also been demonstrated for the Ni site in CO dehydrogenase.[14] Methyl-S-coenzyme-M reductase contains a nickel tetrapyrrole cofactor (F_{430})[15] that exists in both planar and axially ligated forms.[16] None of these biological Ni sites has been characterized crystallographically, and thus, X-ray absorption spectroscopy (XAS) has played a central role in obtaining structural information regarding the Ni sites. Analysis of extended X-ray absorption fine structure (EXAFS) has been used to obtain bond lengths and identify the ligand donor atoms.[10a-c] Studies of the K-absorption edge and X-ray absorption near-edge structure (XANES) have been used to obtain geometrical information about the Ni sites and to study oxidation state changes in the H_2ase Ni site.[17] These studies rely on a relatively small number of generally homoleptic (a complex with identical ligands) and high-symmetry Ni(II) model compounds. Herein, we explore the effects of low symmetry and mixed donor atom environments on the Ni(II) XANES spectra and the ability to obtain information regarding coordination geometry and ligand environment from K-edge data. Particular attention is paid to five-coordinate complexes, where existing data is expanded to include both pyramidal and trigonal-bipyramidal ideal geometries. A series of pairs of isoleptic (complexes with the same ligands) Ni(II/III) complexes are

[†] Department of Chemistry, University of Massachusetts.
[‡] Program in Molecular and Cellular Biology, University of Massachusetts.
[§] Department of Chemistry, University of Connecticut.
[∥] Institute of Molecular Science, University of Connecticut.
[⊥] Department of Chemical Engineering, University of Connecticut.
[#] Department of Chemistry, University of California.

(1) Dixon, N. E.; Gazzola, C.; Blakely, R. L.; Zerner, B. *J. Am. Chem. Soc.* **1975**, *97*, 4131.
(2) Lancaster, J. R., Jr. *Science* **1982**, *216*, 1324.
(3) (a) Cammack, R.; Fernandez, V. M.; Schneider, K. In *The Bioinorganic Chemistry of Nickel*; Lancaster, J. R., Ed.; VCH: Deerfield Beach, FL, 1988; Chapter 8. (b) Moura, J. J. G.; Tiexera, M.; Moura, I.; LeGall, J. *Ibid.*, Chapter 9. (c) Bastian, N. R.; Wink, D. A.; Wackett, L. P.; Livingston, D. J.; Jordan, L. M.; Fox, J.; Orme-Johnson, W. H.; Walsh, C. T. *Ibid.*, Chapter 10.
(4) Ragsdale, S. W.; Wood, H. G.; Morton, T. A.; Ljungdahl, L. G.; DerVartanian, D. V. In *The Bioinorganic Chemistry of Nickel*; Lancaster, J. R., Ed.; VCH: Deerfield Beach, FL, 1988; Chapter 14.
(5) Pfaltz, A. In *The Bioinorganic Chemistry of Nickel*; Lancaster, J. R., Ed.; VCH: Deerfield Beach, FL, 1988; Chapter 12.
(6) Andrews, R. K.; Blakeley, R. L.; Zerner, B. In *The Bioinorganic Chemistry of Nickel*; Lancaster, J. R., Ed.; VCH: Deerfield Beach, FL, 1988; Chapter 7.
(7) Clark, P. A.; Wilcox, D. E. *Inorg. Chem.* **1989**, *28*, 1326.
(8) (a) Clark, P. A.; Wilcox, D. E.; Scott, R. A. *Inorg. Chem.* **1990**, *29*, 579. (b) Hasnain, S. S.; Piggott, B. *Biochem. Biophys. Res. Commun.* **1983**, *112*, 279. (c) Alagna, L.; Hasnain, S. S.; Piggott, B.; Williams, D. J. *Biochem. J.* **1984**, *220*, 591.
(9) Fauque, G.; Peck, H. D., Jr.; Moura, J. J. G.; Huynh, B. H.; Berlier, Y.; DerVartanian, D. V.; Teixeira, M.; Przybyla, A. E.; Lespinat, P. A.; Moura, I.; LeGall, J. *FEMS Microbiol. Rev.* **1988**, *54*, 299.
(10) (a) Lindahl, P. A.; Kojima, N.; Hausinger, R. P.; Fox, J. A.; Teo, B. K.; Walsh, C. T.; Orme-Johnson, W. H. *J. Am. Chem. Soc.* **1984**, *106*, 3062. (b) Scott, R. A.; Wallin, S. A.; Czechowski, M.; Dervartanian, D. V.; LeGall, J.; Peck, H. D., Jr.; Moura, I. *J. Am. Chem. Soc.* **1984**, *106*, 6864. (c) Scott, R. A.; Czechowski, M.; DerVartanian, D. V.; LeGall, J.; Peck, H. D., Jr.; Moura, I. *Rev. Port. Quim.* **1985**, *27*, 67. (d) Albracht, S. P. J.; Kröger, A.; van der Zwaan, J. W.; Unden, G.; Böcher, R.; Mell, H.; Fontijn, R. D. *Biochim. Biophys. Acta* **1986**, *874*, 116.
(11) He, S. H.; Teixeira, M.; LeGall, J.; Patil, D. S.; Moura, I.; Moura, J. J. G.; DerVartanian, D. V.; Huynh, B. H.; Peck, H. D., Jr. *J. Biol. Chem.* **1989**, *264*, 2678.
(12) Eidsness, M. K.; Scott, R. A.; Prickril, B. C.; DerVartanian, D. V.; LeGall, J.; Moura, I.; Moura, J. J. G.; Peck, H. D., Jr. *Proc. Natl. Acad. Sci. U.S.A.* **1989**, *86*, 147.
(13) (a) Cammack, R.; Kovacs, K. L.; McCracken, J.; Peisach, J. *Eur. J. Biochem.* **1989**, *182*, 363-6. (b) Chapman, A.; Cammack, R.; Hatchikian, C. E.; McCracken, J.; Peisach, J. *Febs Lett.* **1988**, *242*, 134. (c) Tan, S. L.; Fox, J. A.; Kojima, N.; Walsh, C. T.; Orme-Johnson, W. H. *J. Am. Chem. Soc.* **1984**, *106*, 3064.
(14) (a) Cramer, S. P.; Eidsness, M. K.; Pan, W.-H.; Morton, T. A.; Ragsdale, S. W.; DerVartanian, D. V.; Ljungdahl, L. G.; Scott, R. A. *Inorg. Chem.* **1987**, *26*, 2477. (b) Bastian, N. R.; Diekert, G.; Niederhoffer, E. C.; Teo, B.-K.; Walsh, C. T.; Orme-Johnson, W. H. *J. Am. Chem. Soc.* **1988**, *110*, 5581.

0020-1669/91/1330-0920$02.50/0

examined by XANES in order to test the transfer of structural information obtained from Ni(II) models to formally Ni(III) complexes and, in conjunction with X-ray photoelectron spectroscopic (XPS) data, to examine the reliability of the X-ray absorption edge energy shifts as an indication of metal-centered redox chemistry. The information obtained from the study of the model compounds is then used to examine the geometry and first coordination sphere ligand environment of the Ni center in *Thiocapsa roseopersicina* hydrogenase.

Experimental Section

Sample Preparation. *T. roseopersicina* H_2ase was isolated from bacteria grown on a modified Pfennig's medium under standard photosynthetic conditions.[18] The bacteria were isolated by centrifugation and stored as a cell paste at −20 °C. The enzyme was isolated and purified by using a minor variation of published procedures[19] and assayed by monitoring H_2 production in the presence of reduced methyl viologen by gas chromatography[20] and using the absorbance at 220 nm as a measure of protein concentration with bovine serum albumin as a standard. Final purification of H_2ase was achieved by preparative gel electrophoresis. Overall yield from 140 g of acetone powder[21] was 20 mg of homogeneous H_2ase. The enzyme sample used in the XAS experiments was prepared in 20 mM Tris-HCl buffer (pH 8) that was 20% glycerol prior to concentration to 0.28 mM. The concentrated sample was poised in form C, using EPR at 77 K to monitor the redox state of the enzyme. The enzyme was first fully reduced by exposure to H_2 overnight (no EPR signal) and was then oxidized back to form C (EPR active) by the addition of a negligible volume of a concentrated anaerobic solution of oxidized benzyl viologen to a final concentration of 2 mM. With this method, a sample containing very nearly 100% of the enzyme in form C can be prepared. Integration of the EPR signal from this sample gave a concentration of 0.27 mM spins,[22] or 0.96 spins/protein, indicating that essentially all of the Ni is in the same redox state.

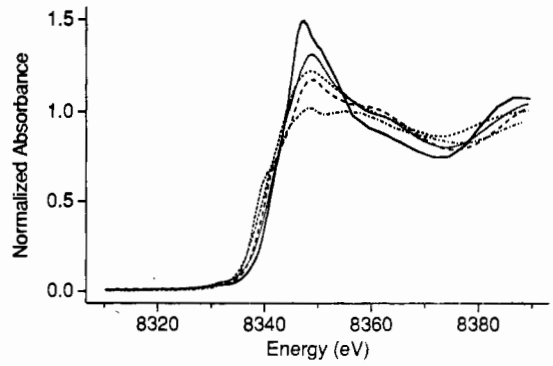

Figure 1. Variation of Ni XANES spectra of six-coordinate complexes with nature of the ligand donor atoms: $[Ni(Im)_6](BF_4)_2$ (**2**), N_6 (—); $Ni(bpy)_2(SPh)_2$ (**7**), N_4S_2 (···); $Et_4N[Ni(S_2Py)_3]$ (**8**), N_3S_3 (- - -); $(Et_4N)_2[Ni(pdtc)_2]$ (**10**), N_2S_4 (– – –); $[Ni(ttcn)_2](BF_4)_2$ (**12**), S_6 (- · -).

Model compounds used in this work are referred to by numbers that are assigned in Table I, which also contains references to the synthetic procedures employed to obtain all previously characterized compounds and to the structures of compounds that have been characterized by crystallography. Solutions of the formally Ni(III)-containing species **30** ($Ni(N_2O_2)^-$) and **34** ($Ni(N_2S_2)^-$) were produced by controlled-potential electrolysis of ca. 2 mM (in Ni) DMF solutions as described in the literature.[39] The pyridine adducts, **13** and **24**, were prepared by addition

(15) Won, H.; Olson, K. D.; Wolfe, R. S.; Summers, M. F. *J. Am. Chem. Soc.* **1990**, *112*, 2178.
(16) (a) Shiemke, A. K.; Scott, R. A.; Shelnutt, J. A. *J. Am. Chem. Soc.* **1988**, *110*, 1645. (b) Shiemke, A. K.; Hamilton, C. L.; Scott, R. A. *J. Biol. Chem.* **1988**, *263*, 5611–6. (c) Hamilton, C. L.; Scott, R. A.; Johnson, M. K. *J. Biol. Chem.* **1989**, *264*, 11605. (d) Shiemke, A. K.; Shelnutt, J. A.; Scott, R. A. *J. Biol. Chem.* **1989**, *264*, 11236. (e) Shiemke, A. K.; Kaplan, W. A.; Hamilton, C. L.; Shelnutt, J. A.; Scott, R. A. *J. Biol. Chem.* **1989**, *264*, 7276. (f) Zimmer, M.; Crabtree, R. H. *J. Am. Chem. Soc.* **1990**, *112*, 1062.
(17) Eidsness, M. K.; Sullivan, R. J.; Cramer, S. P.; Scott, R. A. In *The Bioinorganic Chemistry of Nickel*; Lancaster, J. R., Ed.; VCH: Deerfield Beach, FL, 1988; Chapter 4.
(18) (a) Pfennig, N. *Annu. Rev. Microbiol.* **1974**, *21*, 286. (b) Bogorov, L. V. *Microbiologiya* **1974**, *43*, 326.
(19) Kovacs, K. L.; Tigyi, G.; Alfonz, H. *Prep. Biochem.* **1985**, *15*, 321.
(20) Bagyinka, C.; Zorin, N. A.; Kovacs, K. L. *Anal. Biochem.* **1984**, *142*, 7.
(21) Acetone powder refers to proteins that were precipitated by using cold acetone and dried under vacuum. For details, see ref 19.
(22) Integrations were performed by using DMF solutions of $[Bz(Ph)_3P]$-$[Ni(pdtc)_2]$ as a standard. Our experience integrating solutions of Cu^{II}(EDTA) with this standard gave values for the number of spins (concentration of Cu) that were too high by 10–40%. Thus, using Cu^{II}(EDTA) as an integration standard for H_2ase Ni signals would be expected to underestimate the amount of EPR-detectable Ni present.
(23) Chemical abbreviations used are as follows: bimp, 2,6-bis[((bis((1-methylimidazol-2-yl)methyl)methyl)amino)ethyl]-4-methylphenolate; bpy, 2,2′-bipyridine; sal, salicylaldehyde; Im, imidizole; ttcn, 1,4,7-trithiacyclononane; cyclam, 1,4,8,11-tetraazacyclodecane; SPh, thiophenolate; tren, tris(2-aminoethyl)amine; Me_6tren, tris(2-(dimethylamino)ethyl)amine; pdtc, pyridine-2,6-bis(thiocarboxylate); Py2S, pyridine-2-thiolate; Pm2S, pyrimidine-2-thiolate; N_2O_2, *N,N′*-ethylenebis(*o*-hydroxybenzimide); pp3, tris(2-(diphenylphosphino)-ethyl)phosphine; np_3, tris(2-(diphenylphosphino)ethyl)amine; cyclops, 1,1-difluoro-4,5,11,12-tetramethyl-1-bora-3,6,10,13-tetraaza-2,14-dioxacyclotetradeca-3,5,10,12-tetraenate; dmpn, *N,N′*-dimethyl-*N,N′*-bis(2-mercaptoethyl)-1,3-propanediamine; N_2S_2, *N,N′*-ethylenebis(*o*-mercaptobenzamide); p_3, 1,1,1-tris((diphenylphosphino)methyl)ethane; salen, *N,N′*-ethylenebis(salicylideneaminato); SS_2, bis(2-mercaptoethyl) sulfide; TPP, *meso*-tetraphenylporphyrin; edt, 1,2-ethanedithiolate; mnt, maleonitrile; NS_2SMe, *N,N*-bis(2-mercaptoethyl)-2-(methylthio)-ethylamine; aet, 2-aminoethanethiol; S-*p*-C_6H_4Cl, *p*-chlorothiophenol; MPG, *N*-(2-mercaptopropionyl)glycine; $NSSO_2SMe$, *N*-(2-mercaptoethyl)-*N*-(2-sulfonylethyl)-2-(methylthio)ethylamine; NS-SSMe, *N,N*-3,4-dithiahexane-1,6-diyl(2-(methylthio)ethyl)amine.
(24) Stewart, J. M.; Lingafelter; E. C.; Breazeale, J. D. *Acta Crystallogr.* **1961**, *14*, 888.
(25) Tyson, G. N., Jr.; Adams, S. C. *J. Am. Chem. Soc.* **1940**, *62*, 1228.
(26) Van Ingen Schenau, A. D. *Acta Crystallogr., Sect. B* **1975**, *B31*, 2736.
(27) Reedijk, J. *Recl. Trav. Chim. Pays-Bas* **1969**, *88*, 1451.
(28) Colpas, G. J.; Kumar, M.; Day, R. O.; Maroney, M. J. *Inorg. Chem.* **1990**, *29*, 4779.
(29) Buchanan, R. M.; Mashuta, M. S.; Oberhausen, K. J.; Richardson, J. F.; Li, Q.; Hendrickson, D. N. *J. Am. Chem. Soc.* **1989**, *111*, 4497.
(30) Bosnich, B.; Mason, R.; Paulig, P. J.; Robertson, G. B.; Tobe, M. L. *J. Chem. Soc., Chem. Commun.* **1965**, 97.
(31) Barefield, E. K.; Wagner, F.; Flerlinger, A. W.; Dahl, A. R. *Inorg. Synth.* **1976**, *16*, 220.
(32) Ito, T.; Sugimpoto, M.; Toriumi, K.; Ito, H. *Chem. Lett.* **1981**, 1477.
(33) Chan, P. K.; Poon, C. K. *J. Chem. Soc., Dalton Trans.* **1976**, 858.
(34) Osakada, K.; Yamamoto, T.; Yamamoto, A.; Takenaka, A.; Sasada, Y. *Acta Crystallogr., Sect. C* **1984**, *C40*, 85.
(35) Yamamoto, T.; Sekine, Y. *Inorg. Chim. Acta* **1984**, *83*, 47.
(36) Rosenfield, S. G.; Berends, H. P.; Gelmini, L.; Stephan, D. W.; Mascharak, P. K. *Inorg. Chem.* **1987**, *26*, 2792.
(37) Krüger, H.-J.; Holm, R. H. *J. Am. Chem. Soc.* **1990**, *112*, 2955.
(38) Setzer, W. N.; Ogle, C. A.; Wilson, G. S.; Glass, R. S. *Inorg. Chem.* **1983**, *22*, 266.
(39) Krüger, H. J.; Holm, R. H. *Inorg. Chem.* **1987**, *26*, 3647.
(40) Bertini, I.; Ciampolini, M.; Dapporto, P.; Gatieshi, D. *Inorg. Chem.* **1972**, *11*, 2254.
(41) Ciampolini, M.; Nardi, N. *Inorg. Chem.* **1966**, *5*, 41.
(42) DiVaira, M.; Orioli, P. L. *Acta Crystallogr., Sect. B* **1968**, *24*, 595.
(43) Di Vaira, M.; Midollini, S.; Sacconi, L. *Inorg. Chem.* **1977**, *16*, 1518.
(44) Ghilardi, C. A.; Midollini, S.; Sacconi, L. *Inorg. Chem.* **1975**, *14*, 1790.
(45) Addison, A. W.; Watts, B.; Wicholas, M. *Inorg. Chem.* **1984**, *23*, 813.
(46) Anderson, O. P. *Acta Crystallogr., Sect. B* **1981**, *B37*, 1194.
(47) Mealli, C.; Midollini, S. *Inorg. Chem.* **1983**, *22*, 2286.
(48) Kumar, M.; Day, R. O.; Colpas, G. J.; Maroney, M. J. *J. Am. Chem. Soc.* **1989**, *111*, 5974.
(49) Rothemund, P.; Menotti, A. R. *J. Am. Chem. Soc.* **1948**, *70*, 1808.
(50) Gagnē, R. R.; Ingle, D. M. *Inorg. Chem.* **1981**, *20*, 420.
(51) Stewart, J. M.; Lingerfelter, E. C.; Breazeale, J. D. *Acta. Crystallogr.* **1961**, *14*, 888.
(52) Pfeiffer, P.; Breith, E.; Lubbe, E.; Tsumaki, T. *Ann. Chem.* **1933**, *503*, 84.
(53) Ojima, H. *Nippon Kagaku Zashi* **1967**, *88*, 329.
(54) Jicha, D. C.; Busch, D. H. *Inorg. Chem.* **1962**, *1*, 872.
(55) Tanaka, Y.; Yokoyama, A. *Chem. Pharm. Bull.* **1962**, *10*, 556.
(56) Kumar, M.; Colpas, G. J.; Day, R. O.; Maroney, M. J. *J. Am. Chem. Soc.* **1989**, *111*, 8323.
(57) Baidya, N.; Olmstead, M. M.; Mascharak, P. M. *Inorg. Chem.* **1989**, *28*, 3426.
(58) (a) Barclay, G. A.; McPartlin, E. M.; Stephenson, N. C. *Acta Crystallogr., Sect. B* **1969**, *B25*, 1262. (b) Baker, D. J.; Goodall, D. C.; Moss, D. S. *Chem. Commun.* **1969**, 325.
(59) Mascharak, P. K. Unpublished results.

Table I. Ni k-Edge XAS Data

no.	compd[a]	donor atoms	1s → 3d peak area, 10^{-2} eV[c]	edge energy, eV[d]	hardness[d]	edge slope[d]	max intens[d]	ref cryst struct[e]	ref synth
			Six-Coordinate Complexes						
1	$[Ni(sal)_2(H_2O)_2]$	O_6	4.0	8341.6	6.53	0.19	1.63	24	25
2	$[Ni(Im)_6](BF_4)_2$	N_6	3.9	8341.6	6.90	0.16	1.49	26	27
3	$[Ni(tren)_2](BF_4)_2$	N_6	1.0	8341.3	6.90	0.13	1.31	28	28
4	$[Ni_2(bimp)(OAc)_2]ClO_4$	N_3O_3	3.4	8341.7	6.48	0.16	1.39	29	29
5	$Ni(cyclam)Cl_2$	N_4Cl_2	1.1	8340.1	6.16	0.13	1.17	30	31
6	$[Ni(cyclam)Cl_2]ClO_4$	N_4Cl_2	1.7	8340.6	6.16	0.11	1.22	32	33
7	$Ni(bpy)_2(SPh)_2$	N_4S_2	1.8	8340.6	5.97	0.12	1.31	34	35
8	$Et_4N[Ni(Py2S)_3]$	N_3S_3	1.8	8339.4	5.50	0.11	1.22	36	36
9	$Et_4N[Ni(Pm2S)_3]$	N_3S_3	1.9	8339.3	5.50	0.11	1.21	36	36
10	$(Et_4N)_2[Ni(pdtc)_2]$	N_2S_4	2.3	8340.1	5.03	0.11	1.17	37	37
11	$BzPh_3P[Ni(pdtc)_2]$	N_2S_4	3.9	8340.7	5.03	0.10	1.12	37	37
12	$[Ni(ttcn)_2](BF_4)_2$	S_6	1.7	8339.8	5.30	0.10	1.02	38	38
13	$Et_4N[Ni(N_2O_2)(py)_2]$[b]	N_4O_2	0.6	8342.7	6.47	0.11	1.16		39
			Five-Coordinate Complexes						
			Trigonal-Bipyramidal Geometry						
14	$[Ni(Me_6tren)NCS]NCS$	N_5	4.2	8341.5	6.58	0.12	1.25	40	41
15	$[Ni(Me_6tren)Cl]Cl$	N_4Cl	9.6	8341.1	6.46	0.13	1.19	(28)	41
16	$[Ni(Me_6tren)Br]Br$	N_4Br	6.7	8340.6	6.36	0.12	1.24	42	41
17	$[Ni(np_3)SH]BPh_4$	NP_3S		8339.4	5.20	0.10	1.11		43
18	$[Ni(pp_3)SH]BPh_4$	P_4S	6.5	8339.0	4.82	0.09	1.08	43	43
19	$[Ni(pp_3)H]BF_4$	P_4H	8.9	8339.5	5.36	0.10	1.16		44
			Pyramidal Geometry						
20	Ni(cyclops)Br	N_4Br	6.7		6.36		1.29		45
21	Ni(cyclops)I	N_4I			6.26		1.18	46	45
22	$[Ni(p_3)S]_2ClO_4$	P_3S_2			4.64		1.02	47	47
23	$[Ni(NS\text{-}SSMe)I_2]$	NS_2I_2	6.0		4.50		1.20	48	48
24	$Et_4N[Ni(N_2S_2)py]$[b]	N_3S_2	4.2		5.97		1.05		39
			Four-Coordinate Complexes						
			Planar Geometry						
25	Ni(TPP)	N_4	0.9	8342.9	6.10		1.17		49
26	$[Ni(cyclops)]ClO_4$	N_4	2.3		6.90		1.21		50
27	$[Ni(cyclam)](ClO_4)_2$	N_4	2.0		6.90		1.07		31
28	Ni(salen)	N_2O_2	<0.5		6.25		1.11	51	52
29	$(Et_4N)_2[Ni(N_2O_2)]$	N_2O_2	<0.5	8340.6	5.45		1.12		39, 53
30	$Et_4N[Ni(N_2O_2)]$[b]	N_2O_2	<0.5	8341.9	5.45		1.08		39
31	Ni(dmpn)	N_2S_2	2.9		5.50		0.91	28	28
32	$Ni(aet)_2$	N_2S_2	1.4		5.50		1.08		54
33	$(Et_4N)_2[Ni(N_2S_2)]$	N_2S_2	<0.5	8339.3	4.70		0.99		55
34	$Et_4N[Ni(N_2S_2)]$[b]	N_2S_2	<0.5	8340.5	4.70		1.04		39
35	$Et_4N[Ni(NSSO_2SMe)CN]$	NS_2C	2.4		5.40		1.00	56	56
36	$(NH_4)_3[Ni(MPG)]_3$	NOS_2	<0.5		5.18		1.21	57	57
37	$[Ni(NS_2SMe)]_2$	NS_3	1.8		4.80		0.96	28	28
38	$[Ni(SS_2)]_2$	S_4	2.0		4.40		0.93	58	58
39	$(PPh_4)_2[Ni(edt)_2]$	S_4	<0.5	8338.9	4.10		0.98	59	59
40	$(Et_4N)_2[Ni(mnt)_2]$	S_4	<0.5	*f*	4.10		0.91	(60)	61
41	$Et_4N[Ni(mnt)_2]$	S_4	<0.5	*f*	4.10		0.97	60	62
			Tetrahedral Geometry						
42	$(Me_4N)_2[NiCl_4]$	Cl_4	11.4	8340.0	4.70		1.21	63	64
43	$(Et_4N)_2[Ni(S\text{-}p\text{-}C_6H_4Cl)_4]$	S_4	10.5	8338.2	4.10		1.03	65	65
44	$\{[Ni(p_3)]_2S\}(BPh_4)_2$	P_3S	8.0	8340.6	4.78		1.05	66	66

[a] The abbreviations used are defined in ref 21. [b] Data taken in fluorescence mode. [c] Error estimated to be ±0.005 on the basis of the analysis of noise, Lorentzian fits of the peaks, and background corrections. The background correction constitutes the largest contribution to the error. [d] See definitions in text. [e] References in parentheses are structures of the same Ni-containing species with different counterions. [f] The mnt complexes are the only redox pair where the absorption edges for the formally Ni(III) and Ni(II) complexes cross each other. This fact indicates that the value of ΔE is ca. 0 eV, even though the edge energies cannot be accurately determined because of edge structure that interferes at a normalized absorbance of 0.5.

of 20% by volume of pyridine to the electrochemically oxidized samples. EPR spectra taken before and after exposure to synchrotron radiation demonstrate the identity of each species in solution and its stability under experimental conditions.

Data Collection. Ni K-edge X-ray absorption data were collected over several periods on beam line X-9A at NSLS, with the exception of compounds (**8**, **9**, **15**, **36**, **38**) that were run at CHESS. Data collection at NSLS was under dedicated conditions at ca. 2.53 GeV and 60–120 mA, using a Si(111) double-crystal monochromator that was calibrated by using the first inflection point of Ni foil (8331.6 eV). This arrangement provided a theoretical resolution of ca. 1 eV at 8.3 keV for a 1-mm

(60) Kobayashi, A.; Sasaki, Y. *Bull. Chem. Soc. Jpn.* **1977**, *50*, 2650.
(61) Gray, H. B.; Williams, R.; Bernal, I.; Billig, E. *J. Am. Chem. Soc.* **1962**, *84*, 3596.
(62) Davison, A.; Edelstein, N.; Holm, R. H.; Maki, A. H. *J. Am. Chem. Soc.* **1963**, *85*, 2029.
(63) Wiesner, J. R.; Srivastava, R. C.; Kennard, C. H. L.; DiVaira, M.; Lingafelter, E. C. *Acta Crystallogr.* **1967**, *23*, 565.
(64) Gill, N. S.; Taylor, F. B. *Inorg. Synth.* **1967**, *9*, 136.
(65) Rosenfield, S. G.; Armstrong, W. H.; Mascharak, P. M. *Inorg. Chem.* **1986**, *25*, 3014.
(66) Mealli, C.; Midollini, S.; Sacconi, L. *J. Chem. Soc., Chem. Commun.* **1975**, 765.

hutch slit height; however, edge energy calibrations were reproducible to within ±0.2–0.3 eV. Harmonic rejection was accomplished with a focusing mirror left flat (NSLS) or by detuning the monochromator by 50% (CHESS). At NSLS, both external and internal edge calibration methods were used. Internal energy calibration was achieved by measuring the small absorbance observed in I_0 due to the Ni mirror used for harmonic rejection. Data were collected at CHESS under parasitic conditions at stations A-3 and C-2 at 5.2 GeV and 26–49 mA, employing a Si(111) monochromator of similar resolution with identical experimental conditions except as noted above.

Transmission data were collected at room temperature on powdered samples diluted with boron nitride by using N_2 (I_0) and Ar (I) filled ionization chambers. Spectra were typically run at least twice to check for reproducibility. The reported spectra may be a single scan or the sum of two scans. Low-temperature fluorescence data were taken on frozen DMF solutions of compounds **13**, **24**, **30**, and **34** held in thermal contact with liquid N_2 in gold-plated copper sample holders in a cryostat. Fluorescence data were collected by employing an Ar-filled ionization detector equipped with Soller slits and a Co fluorescence filter.[67] The fluorescence spectra reported are the average of 5–9 scans. Fluorescence data were also taken on a sample of *T. roseopersicina* H_2ase that was 0.3 mM in Ni by using a 13-element Ge detector (Canberra). The sample was held at 77 K in a cryostat. The spectra reported are the weighted sums of the data obtained from each element over 20 scans by using the procedure described by Scott.[68]

X-ray photoelectron spectroscopic (XPS) data were obtained on powdered samples with a Leybold-Heraeus LHS-10 surface analysis system with a Mg Kα source (1253.6 eV). The instrument was equipped with a Model RZ 10/11 hemispherical energy analyzer for detection of ejected photoelectrons. Samples were placed on freshly cleaned copper holders and introduced into vacuum slowly to avoid disturbing the sample. Samples were evacuated in a preparatory chamber and then inserted into the analysis chamber and evacuated to pressures in the 10^{-11} Pa range. Survey spectra were collected up to ca. 1000 eV on all samples followed by narrow scans collected on individual elements over 50–100 eV ranges. Detailed spectra were collected by using a fixed analyzer transmission of 150 eV. The spectra were calibrated by setting the C 1s peak visible in all of the samples to 284.6 eV. Binding energies determined in this manner were reproducible to within 0.2 eV with a precision of ±0.05 eV. The spectrometer was calibrated to the Au $4f_{7/2}$ and the Cu $2p_{3/2}$ transitions set at binding energies of 83.8 and 932.4 eV, respectively. No evidence of decomposition of the samples was noticed from replicate scans.

Data Analysis. The edge region of the XAS spectrum was normalized by setting the extrapolated value of a fit to a second-order curve in the region between 8550 and 9200 eV to unity at 8340 eV, with zero extrapolated from a linear fit to the region between 8150 and 8300 eV. A McMaster correction was applied in the edge jump normalization procedure.[69] For spectra that are not complicated by intense preedge features, the energy of the point corresponding to a normalized absorbance of 0.5 was taken as "the edge energy" for comparison purposes. These spectra also allowed an approximation of the "edge slope" to be obtained from a linear regression of the edge between normalized absorbances of 0.2 and 0.8. Areas under the preedge peak assigned to a 1s → 3d transition were determined by a procedure that involves removing the background by fitting the edge and preedge regions to a function composed of linear and arctangent components.[70] The integrated areas of the 1s → 3d transition of the compounds are expressed relative to the integrated area of the peak observed for $(Me_4N)_2[NiCl_4]$. For correlations with ligand "hardness", the hardness of the Ni ligand environment of the model compounds was taken as an average of the absolute hardness of the ligands involved by using the calculations of Parr and Pearson.[71]

Results

The Ni K-edge absorption spectra of several Ni(II) complexes with various mixtures of O, N, and S ligation are shown in Figures 1–3, grouped according to coordination number. A series of six-coordinate complexes with various ratio of N- and S-donor ligands is shown in Figure 1. This figure shows the presence of a peak assigned to a 1s → 3d transition near 8332 eV in every case[72] and illustrates the changes in the shape of the edge that occur as the donor atoms are varied. The shift in the edge energy to lower values that occurs upon substituting O,N ligands with S-donor ligands is also apparent (range = 2 eV). Figure 2 compares the edge features of examples of five-coordinate complexes with idealized trigonal-bipyramidal and square-pyramidal geometries. These two geometries are distinguished in most cases by

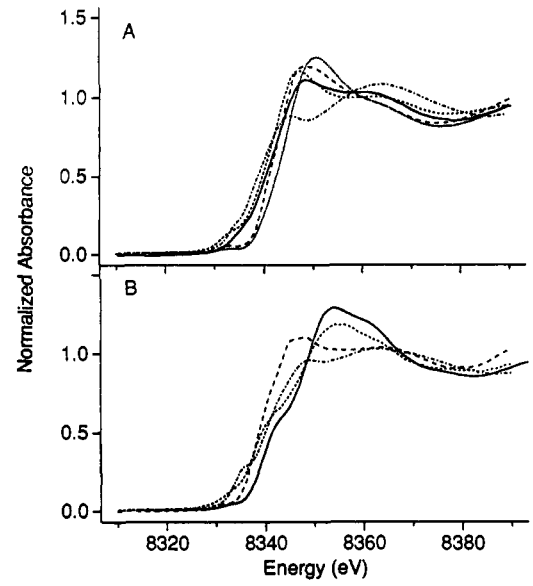

Figure 2. Variation of Ni XANES spectra of five-coordinate complexes as a function of geometry and ligand donor atoms. (A) Trigonal-bipyramidal geometry: $[Ni(Me_6tren)NCS]NCS$ (**14**) (···); $[Ni(Me_6tren)Cl]Cl$ (**15**) (---); $[Ni(np_3)SH]BPh_4$ (**17**) (—); $[Ni(pp_3)SH]BPh_4$ (**18**) (·-·); $[Ni(pp_3)H]BF_4$ (**19**) (-··-). (B) Pyramidal geometry: [Ni(cyclops)Br] (**20**) (—); [Ni(cyclops)I] (**21**) (---); $\{[Ni(p_3)S]_2\}ClO_4$ (**22**) (·-·); $[Ni(NS\text{-}SSMe)I_2]$ (**23**) (-··-).

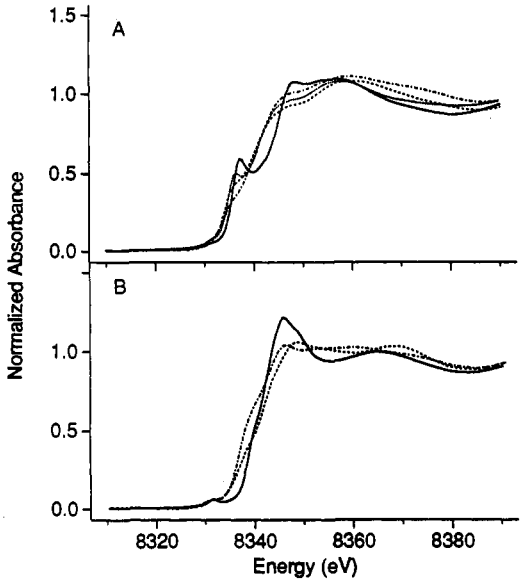

Figure 3. Variation of Ni XANES spectra of four-coordinate complexes as a function of geometry and ligand donor atoms. (A) Planar geometry: $Ni(cyclam)](ClO_4)_2$ (**27**), N_4 (—); [Ni(dmpn)] (**31**), N_2S_2 (···); $[Ni(NS_2SMe)]_2$ (**37**), NS_3 (---); $(Ph_4P)_2[Ni(edt)_2]$ (**39**), S_4 (·-·). (B) Tetrahedral geometry: $Me_4N(NiCl_4)$ (**42**), Cl_4 (—); $(Et_4N)_2[Ni(S\text{-}C_6H_4Cl)_4]$ (**43**), S_4 (·-·); $\{[Ni(p_3)]_2S\}(BPh_4)_2$ (**44**), P_3S (---).

(67) (a) Stearn, E. A.; Heald, S. M. *Rev. Sci. Instrum.* **1979**, *50*, 1579. (b) Lytle, F. W.; Greegor, R. B.; Sandstrom, D. R.; Marques, E. C.; Wong, J.; Spiro, C. L.; Huffman, G. P.; Huggins, P. E. *Nucl. Instrum. Meth. Phys. Res.* **1984**, *226*, 542.
(68) Scott, R. A. *Meth. Enzymol.* **1985**, *117*, 414.
(69) McMaster, W. H.; Kerr Del Grande, N.; Mallet, J. H.; Hubbell, J. H. *Compilation of X-ray Cross Sections*; National Technical Information Service, U.S. Chamber of Commerce: Springfield, VA, 1969; UCRL-50174 Sec. II, Rev. 1.
(70) Roe, A. L.; Schneider, D. J.; Mayer, R. J.; Pyrz, J. W.; Widom, J.; Que, L., Jr. *J. Am. Chem. Soc.* **1984**, *106*, 1676.
(71) Parr, R. G.; Pearson, R. G. *J. Am. Chem. Soc.* **1983**, *105*, 7512.
(72) (a) Schulman, R. G.; Yafet, Y.; Eisenburger, P.; Blumberg, W. E. *Proc. Natl. Acad. Sci. U.S.A.* **1976**, *73*, 1384. (b) Hahn, J. E.; Scott, R. A.; Hodgson, K. O.; Doniach, S.; Desjardins, S. E.; Soloman, E. I. *Chem. Phys. Lett.* **1982**, *88*, 595.

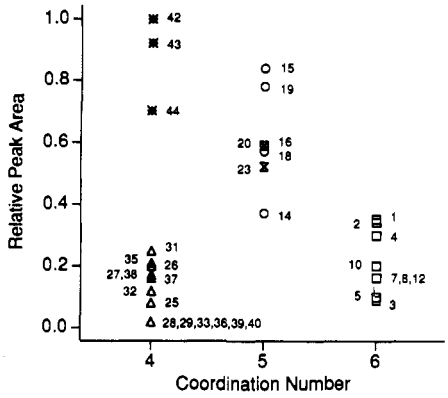

Figure 4. Relative areas under 1s → 3d preedge peaks as a function of coordination number: □ = six-coordinate complexes; X = five-coordinate, pyramidal complexes; ○ = five-coordinate, trigonal-bipyramidal complexes; △ = four-coordinate, planar complexes; ✱ = four-coordinate, tetrahedral complexes. (Numbers refer to compounds in Table I.)

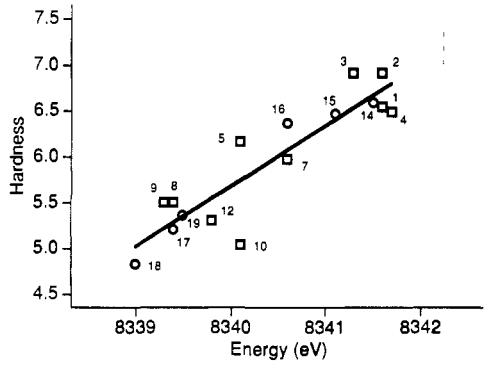

Figure 5. Relationship between the average hardness of the ligands and the Ni k-edge energy: □ = six-coordinate complexes; ○ = five-coordinate, trigonal-bipyramidal complexes. (Numbers refer to Table I.)

a shoulder near 8338 eV that is observed in square-pyramidal geometry but not in trigonal-bipyramidal complexes. This shoulder is due to an absorbance that has been assigned to a 1s → $4p_z$ transition (with shakedown contributions) that is observed in tetragonal geometries, where one or more axial ligands are absent.[73] The five-coordinate complexes also exhibit a 1s → 3d transition near 8332 eV. Figure 3 illustrates the clear differences in edge structure that are exhibited by four-coordinate complexes with idealized planar and tetrahedral geometry. Spectra obtained for planar complexes exhibit a weak 1s → 3d transition and often have a resolved maximum associated with the 1s → $4p_z$ transition.[17] In contrast, tetrahedral complexes have featureless edges but display more intense 1s → 3d transitions.[17] The combination of a weak 1s → 3d absorption and a low edge energy in planar complexes with two or more S-donor ligands frequently obscures the preedge peak associated with this transition.

The 1s → 3d transition is symmetry-forbidden in centrosymmetric point groups but is expected to gain intensity in geometries where p–d mixing can occur.[70] Thus, the intensity of the peak associated with this transition provides another indicator of geometry. Figure 4 shows the relationship between the peak area and coordination number. The numerical values of the areas are shown in Table I. These values are seen to form clusters of points around a particular coordination number. There is no obvious relationship between low- and high-symmetry complexes of a given coordination number and the area of the preedge peak. However, relatively large differences exist between the areas characteristic of different coordination geometries/numbers.

(73) (a) Smith, T. A.; Penner-Hahn, J. E.; Berding, M.; Doniach, S.; Hodgson, K. O. *J. Am. Chem. Soc.* **1985**, *107*, 5945. (b) Bair, R. A.; Goddard, W. A. *Phys. Rev. B* **1980**, *22*, 2767. (c) Kosugi, N.; Yokohama, T.; Asakura, K.; Kuroda, H. *Chem. Phys.* **1984**, *91*, 249. (d) Yokoyama, T.; Kosugi, N.; Kuroda, H. *Chem. Phys.* **1986**, *103*, 101.

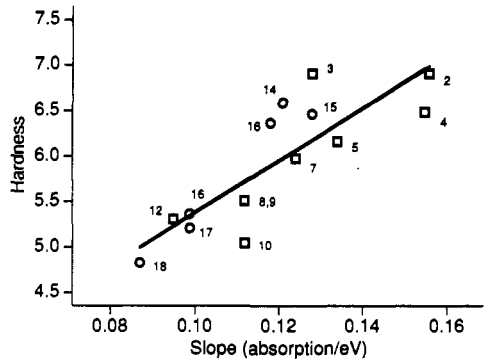

Figure 6. Relationship between the slope (breadth) of the edge and the hardness of the ligands: □ = six-coordinate complexes; ○ = five-coordinate, trigonal-bipyramidal complexes. (Numbers refer to Table I.)

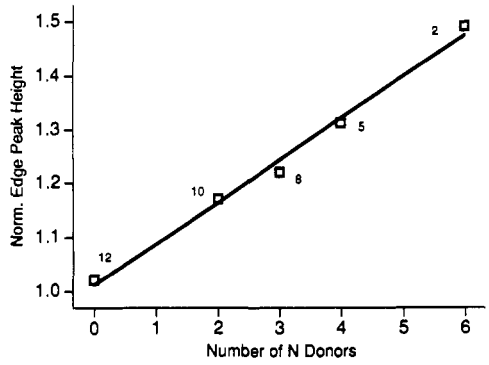

Figure 7. Relationship between maximum normalized intensity of the edge and the ligand environment in six-coordinate complexes with N- and S-donor ligands. (Numbers refer to Table I.)

Table II. Binding Energies for Ni and Donor Atom Electrons

		Energy, eV			
no.	compd	Ni $2p_{1/2}$	Ni $2p_{3/2}$	S 2p or Cl 2p	N 1s
5	$Ni(cyclam)Cl_2$	872.1	854.4	196.9 (Cl)	398.7
6	$[Ni(cyclam)Cl_2](ClO_4)$	872.7	855.3	196.9 (Cl)	398.9
10	$(Et_4N)_2[Ni(pdtc)_2]$	871.0	853.6	161.1 (S)	398.9
11	$(BzPPh_3)[Ni(pdtc)_2]$	871.7	854.3	161.6 (S)	398.9
40	$(Me_4N)_2[Ni(mnt)_2]$[82]		855.5	163.7 (S)	
41	$Me_4N[Ni(mnt)_2]$[82]		855.8	164.4 (S)	
33	$(Et_4N)_2[Ni(N_2S_2)]$	871.2	853.7	161.7 (S)	397.9
29	$(Et_4N)_2[Ni(N_2O_2)]$	871.4	854.1		397.9

The shapes of the Ni K-edges shown in Figures 1–3 indicate that certain features vary in a qualitative, but systematic way, depending on the number of S-donor ligands or high-Z ligands that can be viewed as "soft" ligands according to hard/soft acid/base (HSAB) theory.[74] These edge shape variations include the maximum normalized intensity of the edge region, the edge energy, and the slope of the edge, all of which decrease with increasing numbers of S-donor ligands. The systematic variation of these features with the nature of the ligand environment is illustrated in Figures 5–7 for complexes whose edges are uncomplicated by the presence of a 1s → $4p_z$ transition.

In addition to the results obtained for Ni(II) complexes described above, the edge structures of several Ni(III) compounds have also been examined. This was done partly to test the validity of using data obtained for Ni(II) structures to infer geometric information regarding the structure of Ni(III) centers, such as those postulated for oxidized forms of Ni centers in H_2ases and CO dehydrogenase. Figure 8 compares the Ni K-edges observed for several pairs of isoleptic Ni(II,III) complexes. These spectra reveal only small edge shifts associated with oxidation of Ni(II) complexes. Figure 9 shows spectra taken on solutions of Ni(III)

(74) Pearson, R. G. *Survey of Progress in Chemistry*; Scott, I. A., Ed.; Academic Press: New York, 1969; Volume 1, Chapter 1.

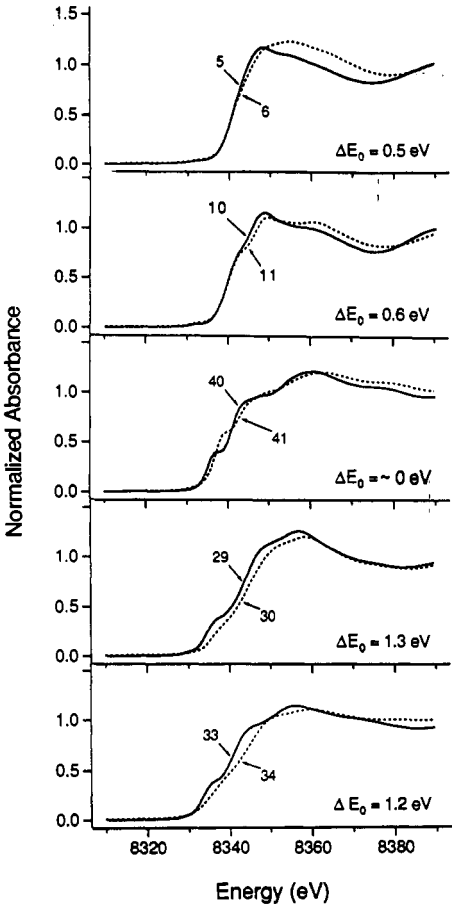

Figure 8. Edge energy shifts occurring upon oxidation in isoleptic Ni(II/III) pairs. (Numbers refer to Table I.)

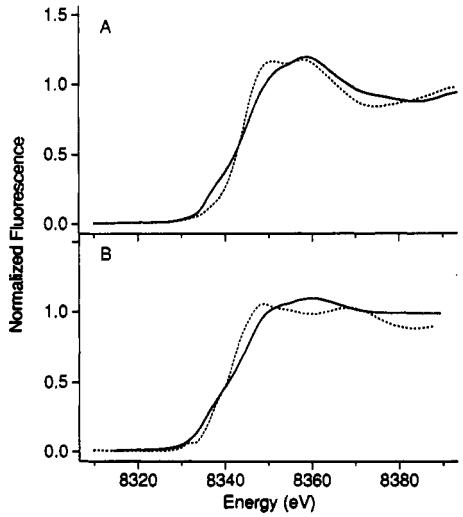

Figure 9. Comparison of Ni(III) edges for complexes upon conversion from four-coordinate planar geometry to six- or five-coordinate complexes: (A) $[Ni(N_2O_2)]^-$ (**30**) (—), $[Ni(N_2O_2)(py)_2]^-$ (**13**) (---); (B) $[Ni(N_2S_2)]^-$ (**34**) (—), $[Ni(N_2S_2)(py)]^-$ (**24**) (---).

complexes upon conversion from four-coordinate to five- or six-coordinate species. These data indicate that the edge features that are useful indicators of geometry for Ni(II) complexes are useful for Ni(III) as well, although the features are broader and less distinct. Areas calculated for 1s → 3d transitions of Ni(III) complexes are ca. 50% larger than those of the corresponding Ni(II) complexes.

Binding energies for Ni and the ligand donor atoms also provide some insight into changes in edge energy as a function of oxidation state and ligand environment. Data relevant to these relationships are found in Table II.

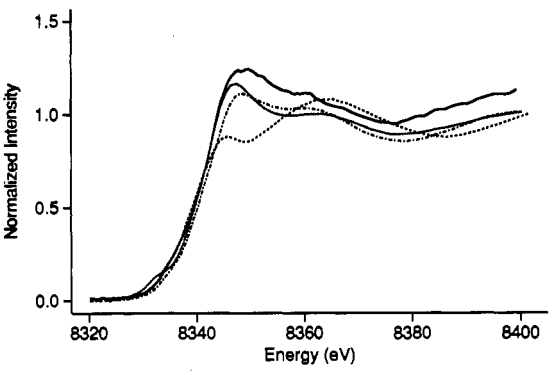

Figure 10. Ni XANES spectrum obtained for *T. roseopersicina* hydrogenase and a comparison with complexes with distorted trigonal-bipyramidal geometry: *T. roseopersicina* H_2ase, form C (—); $[Ni(np_3)SH]BPh_4$ (**17**), NP_3S (···); $[Ni(pp_3)H]BF_4$ (**19**), P_4H (···); $[Ni(pp_3)SH]BPh_4$ (**18**), P_4S (---).

The Ni K-edge spectrum obtained for *T. roseopersicina* hydrogenase is shown in Figure 10. The edge obtained for this biological Ni site does not show any resolvable features associated with either a 1s → 3d or 1s → $4p_z$ transition. Comparison of the edge from the hydrogenase with those obtained from the model compounds reveals that it most closely resembles edges obtained from distorted trigonal-bipyramidal complexes. The edge energy and shape are consistent with a mixed-donor ligand environment like that proposed on the basis of analysis of the EXAFS spectrum.[75]

Discussion

A. Ni XANES and Geometry. The XANES regions of the X-ray absorption spectra of first-row transition-metal complexes have been analyzed by using a combination of theoretical and experimental techniques in order to understand the origin of the observed features.[68,76] In the case of Ni(II), two features have been assigned to specific electronic transitions.[17] A peak observed at approximately 8–9 eV below the edge has been assigned to a 1s → 3d transition, and a peak or shoulder that is observed in tetragonal complexes lacking one or more axial ligands (four-coordinate planar or five-coordinate pyramidal geometries) that occurs 1–3 eV below the edge has been assigned to a 1s → $4p_z$ transition with shakedown contributions. The 1s → 3d transition is a forbidden transition in centrosymmetric point groups but is expected to gain intensity due to p–d mixing in noncentrosymmetric geometries.[70] This would be expected to lead to relatively small peaks associated with six-coordinate and four-coordinate planar geometries and a relatively intense absorption for tetrahedral complexes. It would also predict a range of peak areas for a given coordination number, dependent on the amount of p–d mixing allowed by the geometries involved. The combination of the presence or absence of a 1s → $4p_z$ transition and the apparent intensity of the 1s → 3d transition has been employed to predict the geometry of Ni in several model compounds.[17] These compounds are mostly simple complexes with only one set of donor atoms. We find that these geometry predictions are readily extended to Ni(II) complexes with mixed-ligand environments and to five-coordinate complexes in both idealized trigonal-bipyramidal and pyramidal geometries (Figures 1–3).

Figure 4 shows the areas of the peaks assigned to 1s → 3d transitions in a number of compounds, relative to the area obtained for the peak observed in the spectrum of $(Me_4N)_2[NiCl_4]$. It is clear that the points fall into regions that are characteristic of

(75) Maroney, M. J.; Colpas, G. J.; Bagyinka, C. *J. Am. Chem. Soc.* **1990**, *112*, 7067.
(76) (a) Alema, S.; Bianconi, A.; Castellani, L.; Fasella, P.; Giovannelli, A.; Mobillo, S.; Oesch, B. *J. Mol. Biol.* **1983**, *165*, 125. (b) Durham, P. J.; Pendry, J. B.; Hodges, C. H. *Solid State Commun.* **1981**, *38*, 159. (c) Durham, P. J. *X-ray Absorption: Principles, Applications, Techniques of EXAFS, SEXAFS, and XANES*; Koningsberger, D. C., Prins, R., Eds.; John Wiley and Sons: New York, 1988; Chapter 2. (d) Bianconi, A. *Ibid.*, Chapter 11.

each coordination number and that the relative area can also distinguish between planar and tetrahedral four-coordinate idealized geometries. These two four-coordinate geometries lie at the extremes of the areas observed for the 1s → 3d peaks. Planar complexes feature weak absorbances with relative peak areas falling into the 0.0–0.23 range, while the peaks observed for complexes of more tetrahedral geometry fall in the range 0.70–1.0. The six-coordinate complexes display relatively featureless absorption edges with weak 1s → 3d transitions (Figure 1). The relative peak areas observed for Ni(II) six-coordinate complexes fall in a range 0.09–0.35 (Figure 4). This range is similar to the range observed for four-coordinate planar complexes and indicates that these two geometries cannot be distinguished by this criterion alone. However, Figure 3 reveals that spectra of planar complexes feature a strong absorption at ca. 8338 eV (1s → $4p_z$) that is not observed in six-coordinate complexes. Thus, a relative 1s → 3d peak area of ca. 0.2 indicates either a planar four-coordinate or six-coordinate Ni(II) center, which may be further distinguished by the presence or absence of a 1s → $4p_z$ transition. A similar situation exists in five-coordinate geometries. The area under the 1s → 3d peak of both trigonal-bipyramidal and pyramidal complexes falls in the range 0.37–0.83. However, Figure 2 demonstrates that only spectra of pyramidal complexes reveal features associated with a 1s → $4p_z$ transition, while trigonal-bipyramidal complexes have featureless edges similar to six-coordinate complexes. Although the range of the peak areas of five-coordinate complexes is nearly large enough to include the largest areas for six-coordinate complexes and the smallest areas for tetrahedral complexes, most of the five-coordinate complexes center around a peak area of 0.6, which is easily distinguished from the other two coordination numbers.

Within a particular group of compounds (e.g. six-coordinate complexes), there are both high- and low-symmetry examples. However, no clear relationship exists between the local symmetry of the Ni center and the variations in preedge peak areas that are observed. For example, both compounds **2** and **3** are both six-coordinate complexes with nearly octahedral local symmetry but lie at the two extremes of the areas observed for six-coordinate compounds. Similarly, the highly distorted complexes **8** and **9**, with N_3S_3 donor atom sets (ideally C_{2v} symmetry), have areas of 0.16 that are near the average value for six-coordinate compounds (0.20), despite the fact that p–d mixing is allowed in this point group. It is possible that other factors, including the errors arising from the background correction and area calculations, are larger than the variation of p–d mixing that occurs in complexes of different symmetry but similar geometry.

In four-coordinate planar complexes with large numbers of S-donor ligands, it is frequently not possible to observe the peak assigned to a 1s → 3d transition. This arises from the combination of the low intensity of the peak in these compounds, another feature (1s → $4p_z$) near the preedge peak, and the shift to lower edge energy induced by the S-donor ligands. In these cases, predictions of four-coordinate planar or five-coordinate pyramidal geometry are possible but cannot be clearly distinguished. With the exception of four-coordinate planar geometries with two or more S-donor ligands, the determination of geometry using 1s → 3d peak areas in combination with the presence or absence of a 1s → $4p_z$ transition (with shakedown contributions) appears to be an accurate indication of coordination number/geometry that is relatively insensitive to the nature of the ligand donor atoms.

B. Ni XANES and Ligand Environment. Information regarding the nature of the ligand donor atoms in a Ni(II) complex can be obtained from the analysis of other edge features. For example, a general shift to lower edge energies is observed for complexes with increasing numbers of S-donor ligands. This is consistent with the notion that as more polarizable ligands are added to the Ni coordination sphere, the positive charge density on the Ni atom decreases, leaving the center easier to oxidize. This reduction of the effective charge of the Ni center by the ligands is reflected in expressions used to evaluate the effective charge (vide infra). This phenomenon has been observed many times but is difficult to quantitate in compounds with mixed-ligand environments without detailed molecular orbital calculations. However, in a series of Ni(II) compounds we have observed that there is a correlation between the average "hardness" of the ligands, as determined by the Parr and Pearson absolute hardness scale,[71] and the edge energy of six-coordinate and five-coordinate trigonal-bipyramidal complexes, absorption edges that are uncomplicated by 1s → $4p_z$ transitions (Figure 5). This relationship is also apparent in some planar four-coordinate complexes, where the lower energy transition is sufficiently resolved to enable the edge energy to be determined. Thus, the determination of the edge energy helps to place limits on the number of hard and soft donor atoms that can be bound.

Similarly, increasing covalency in metal–ligand bonds leads to an edge broader than that observed for simple N,O-donor ligands.[17] We have defined a crude "edge slope" to be the slope of a linear fit of the edge between normalized absorbance values of 0.2 and 0.8. This region is uncomplicated by additional edge features in all geometries except planar four-coordinate and five-coordinate pyramidal geometries. The slope of an edge from a complex containing only O,N-donor ligands is about twice as steep as that observed for complexes containing only P,S-donor ligands. A plot of the edge slope vs the average hardness of the ligands, shown in Figure 6 for six-coordinate and five-coordinate trigonal-bipyramidal geometries, reveals a trend toward decreasing slope with decreasing hardness. Fits of a smaller part of the edge in four-coordinate planar complexes reveal the same trend, but more scatter in the data exists due to the smaller number of points that are used to determine the edge slope.

The maximum intensity of the edge region of the XANES spectra of Ni(II) complexes is also sensitive to the ligand environment. In Figure 7, a series of six-coordinate complexes with mixed N,S ligation reveals a linear relationship between the number of N-donor (or S-donor) atoms in the first coordination sphere and the maximum normalized absorbance. The trend is for decreasing absorbance with increasing numbers of S-donor ligands. This same trend is observed for complexes with other geometries, although no linear relationship between the number of S-donor ligands and the edge height can be discerned. Clearly, other factors may also contribute to the shape of the absorption edge.

Figure 2 contains an example of a five-coordinate Ni(II) hydride complex (**19**). Comparison of the edge features associated with this complex and the edges of compounds **17** (an NP_3S donor set) and **18** (a P_4S donor set) indicates that the presence of the hydride ligand has roughly the same effect on the spectrum as the substitution of a P-donor by an N-donor (soft for hard). Figure 5 shows that the position of the hydride complex in the energy vs hardness correlation is appropriate for the value of the hardness calculated for the hydride ligand, which is indicative of a hard donor atom. The presence of a hydride ligand clearly has an effect on the edge structure of this Ni complex, although it does not contribute to the EXAFS spectrum.[77]

C. Ni XANES and Oxidation State. Five pairs of isoleptic Ni(II)/(III) complexes were examined in order to investigate the nature of the oxidized Ni complexes and the reliability of information obtained from Ni(II) models applied to Ni(III) complexes. A comparison of the edges obtained for the Ni(II/III) pairs is shown in Figure 8. The shifts in edge energy upon oxidation are small and range from ca. 0 in the case of $Ni(mnt)_2^{2-/-}$ (**40**, **41**) to 1.3 eV in compounds **29** and **30**. It has been shown from theory that the shift in X-ray absorption edge energy (ΔE) is related to the effective nuclear charge seen by an electron on the metal atom in the final level ($Z_{eff}^{m,f}$) and the effective charge (q) on the metal atom by eq 1, where a_f is a constant related to

$$\Delta E = 2a_f Z_{eff}^{m,f} q + a_f q^2 \quad (1)$$

the quantum defect.[78] The charge on the metal atom is not a simple function of formal oxidation state but is also dependent

(77) Maroney, M. J.; Colpas, G. J. Unpublished results.
(78) Sarode, P. R.; Ramasesha, S.; Madhusudan, W. H.; Rao, C. N. R. *J. Phys. C* **1979**, *12*, 2439.

on the nature of the ligands present.[79] In the case of the study cited, q was calculated by the method of Suchet et al. according to eq 2, where Z is the total number of electrons, r is the ionic

$$q = n[1 - 0.01185(Z/r' + Z'/r)] \quad (2)$$

radius, n is the oxidation number of the metal center, and the primed values refer to the analogous quantities for the anion in the binary compounds studied. The operational definition of absolute hardness is half of the difference between ionization potential and electron affinity, quantities related to r' and Z', which constitute the theoretical basis for the correlations with ligand hardness (vide supra) in the absence of a change in formal oxidation state of the metal.

Although ΔE generally increases with formal oxidation state, there is no direct relationship between X-ray absorption edge energy and formal oxidation state. In fact, the edge energy shifts due to one-electron oxidations in this series of Ni(II/III) complexes are significantly less (ca. 33%) than those observed in Ni(II) complexes upon changing the ligands from O,N-donors to S-donors (Table I). Thus, edge energy shifts as a indication of oxidation state changes are meaningless in the absence of specific knowledge of the ligand environment and any changes therein. Instead, shifts in edge energy reflect changes in the effective charge on Ni. This relationship (eq 3) has been demonstrated for Ni complexes in

$$\Delta E = aq + bq^2 \quad (3)$$

formal oxidation states from 0 to IV[80] and has a parabolic form similar to eq 1. In the case of $Ni(mnt)^{2-,-}$ complexes, where little structural change occurs upon oxidation,[60] the lack of a significant shift in the edge energy indicates that little or no increase in charge occurs for Ni in these complexes upon oxidation and is consistent with the notion that the oxidation (loss of electron density) involves an orbital that is largely localized on the ligand. This result is consistent with $X\alpha$ calculations[81] and X-ray photoelectron spectroscopic studies[82] of the electronic structure of these complexes. The larger shifts observed for other complexes (Table II) indicate that oxidation of these complexes involves a molecular orbital with more Ni character. It is worth noting that larger values of ΔE upon oxidation are usually associated with ligands containing mostly O,N-donor atoms.

Additional insights into the electronic structure of the Ni(III) complexes can be obtained by using X-ray photoelectron spectroscopy (XPS). The use of metal 2p binding energies to examine changes in effective charge (q) has advantages over the use of X-ray absorption data. The XPS measurements are not encumbered by the difficulty of determining the edge energy, particularly in the presence of complex edge structure, and should be more sensitive to changes in the number of valence electrons. The XPS technique also allows the binding energy changes of electrons on the ligand donor atoms to be easily determined. That both techniques are measuring changes in effective charge is reflected by the linear relationship observed between values of ΔE from XAS measurements and $2p_{3/2}$ binding energies from XPS.[76,80]

Table II contains the binding energies of the Ni and ligand donor atoms in several complexes. Three pairs of isoleptic Ni(II/III) complexes allow the effect of oxidation state changes to be addressed. In general, a ligand environment composed of largely hard O,N-donor ligands leads to a substantial change in the binding energy of the Ni electrons upon oxidation. The ligand donor atoms are not greatly affected (e.g. **5** and **6**). In contrast, ligand environments featuring S-donor ligands lead to smaller changes in the binding energy of Ni 2p electrons and larger changes in donor atom binding energies. In the case of the mnt ligand, little change in binding energy for the Ni center is observed upon oxidation, while large changes in binding energies of the S-donors are observed. This confirms previous results, which were interpreted as evidence for ligand oxidation in preference to metal-centered oxidation in this compound.[82] With binding energies as a criterion, compounds **10** and **11** represent cases that are closer to Ni-centered oxidation than to ligand-centered oxidation, although changes in the binding energy on S are also apparent. The metal-centered nature of the oxidation of **10** is a natural consequence of the high symmetry of the molecule (unpaired spin density may be delocalized over four equivalent sulfur centers and the Ni atom) and a decrease in the electron-donating properties of thiocarboxylate sulfurs vs alkanethiolates. This latter effect is also apparent in the correlations between edge energy and edge slope with the average ligand hardness (Figures 5 and 6). Figure 5 reveals that the point lying furthest off the least-squares fit of the data is compound **10**, which lies substantially below the line. This is undoubtedly due to the fact that the thiocarboxylate donors are not as soft as the HS^- ligand, whose hardness value was used to compute the hardness of negatively charged S-donor ligands.

Two complexes with similar ligands differing in O- vs S-donor atoms provide some insight into changes in binding energy induced by the donor atoms. As expected, these two compounds show a slightly increased binding energy for Ni in the complex lacking S-donor ligands.

The edges obtained for the Ni(III) complexes are broader than those of the corresponding Ni(II) complexes, indicative of increased covalency. The edge structures useful in determining geometry in Ni(II) complexes are retained in the Ni(III) complexes, although the increased breadth of the edge makes these features less distinct in the Ni(III) complexes. Nonetheless, these features remain accurate indicators of geometry. The Ni(III) compounds **30** and **34** are known to add pyridine ligands in solution to form six-coordinate and five-coordinate pyramidal complexes, respectively.[39] This has been clearly shown by using EPR spectra that reveal hyperfine structure arising from two axial N-donors in the case of **13** and only one axial N-donor in the case of **24**. These changes in coordination are reflected in the edge structures of the compounds (Figure 9). Compound **30** shows the loss of the shoulder associated with the $1s \rightarrow 4p_z$ transition upon adding two pyridine ligands to become six-coordinate. In the case of **34**, the conversion to five-coordination is reflected by a decrease in the intensity of the same feature.

Direct comparison of the areas of the peaks assigned to $1s \rightarrow 3d$ transitions of the two Ni(II/III) pairs where this feature is clearly visible (Table I) reveals that the peak areas for the Ni(III) complexes are roughly 50% bigger than in the corresponding Ni(II) complex. This increase in peak area upon oxidation is expected to occur due to an increase in the number of d-orbital holes from 2 to 3. Similar trends can also be seen between metals. For example, the peak areas obtained from high-spin Fe(III) complexes[70] are 2–3 times larger than the peak areas obtained for Ni(II) complexes of the same geometry. This increase is close to the factor of 2.5 expected for increasing the number of d-orbital holes from 2 to 5. For this reason, the area of the preedge peak cannot be interpreted without knowledge of the oxidation state of the metal center.

D. Application of Ni XANES to the Structure of Ni Sites in Hydrogenase. The edge spectrum shown in Figure 10 was obtained on a sample of *T. roseopersicina* hydrogenase that was poised in form C prior to data collection. Form C is a key intermediate in the reversible oxidation of H_2. It lies two electrons reduced from oxidized (as isolated) forms of the enzyme and displays an $S = {}^1/_2$ EPR signal.[83] This EPR signal has been attributed to a formally Ni(I) center[3a,84] or Ni(III) center,[85] with either possibly

(79) Suchet, J. P.; Bailly, F. *Ann. Chim.* **1965**, *10*, 517.
(80) Manthiram, A.; Sarode, P. R.; Madhusudan, W. H.; Gopalakrishnan, J.; Rao, C. N. R. *J. Phys. Chem.* **1980**, *84*, 2200.
(81) Sano, M.; Adachi, H.; Yamatera, H. *Bull. Chem. Soc. Jpn.* **1981**, *54*, 2636.
(82) Lalitha, S.; Chandramouli, G. V. R.; Manoharan, P. T. *Inorg. Chem.* **1988**, *27*, 1492.
(83) Cammack, R.; Bagyinka, C.; Kovacs, K. L. *Eur. J. Biochem.* **1989**, *182*, 357.
(84) van der Zwaan, J.; Albracht, S. P.; Fontijn, R. D.; Slater, E. C. *Febs Lett.* **1985**, *179*, 271.
(85) Teixeira, M.; Moura, I.; Xavier, A. V.; Huynh, B. H.; DerVartanian, D. V.; Peck, H. D., Jr.; LeGall, J.; Moura, J. J. G. *J. Biol. Chem.* **1985**, *260*, 8942.

involving a hydride[82,83] or dihydrogen ligand.[86] Studies of edge energy shift upon reduction of the Ni center in *Desulfovibrio gigas* H_2ase do not reveal any substantial energy shift until the full reduced state (one electron below form C) is reached,[17] and this shift is on the order of 2 eV. These data suggest that no significant change in the effective charge on Ni occurs upon reduction until the lowest oxidation state of the center is reached. The magnitude of this shift is larger than has been observed in any of the isoleptic Ni(II,III) pairs that we have examined (particularly those with S-donors) and might be more appropriately attributed to a change in ligation. Without additional information, it is not possible to clearly distinguish between these two possibilities. Given the presence of several S-donor ligands in the Ni site (vide supra)[75] and the data presented above, it is unlikely that a substantial change in the electron density of the Ni site from that typical of nickel(II) thiolates occurs during redox cycling of this enzyme. Thus, the use of Ni(II) models to examine the structure of the edge in H_2ase form C is valid, particularly given the presence of the same general structure of Ni(III) edges.

The edge obtained for *T. roseoperisicina* H_2ase form C does not reveal either a peak or a distinct shoulder in the 8338-eV region that would be characteristic of a four-coordinate planar complex. Also, no evidence for a strong 1s → 3d transition is visible near 8332 eV. This rules out a four-coordinate center and leaves as the possibilities both five-coordinate geometry and six-coordinate structures. The lower energy region of the edge does have a significantly different slope, a feature that is strongly reminiscent of edges observed for distorted trigonal-bipyramidal model complexes (Figure 2). A comparison of the edge obtained from the Ni site in the enzyme with those obtained from distorted trigonal-bipyramidal models is shown in Figure 10. The edge obtained for a complex with a P_4S donor set (all soft) is clearly distinct from that obtained for the enzyme. The edges obtained for a distorted trigonal-bipyramidal complex having a NP_3S or P_4H donor atom set (one hard and four soft donors) bear strong resemblances to the XANES spectrum of the enzyme site. The lower maximum absorbance for the model compounds relative to the enzyme probably reflects the presence of more hard donor ligands in the biological site. The edge energy (8339.7 eV) corresponds to an average ligand hardness of 5.35 from the data in Figure 5. This value requires a large number of soft donors and/or negatively charged donors in the Ni coordination sphere. Given the involvement of S-donor ligands detected in the EXAFS spectrum[75] and a five-coordinate geometry, the hardness is closest to a value of 5.26 calculated for a complex composed of two thiolates, two anionic O-donors, and one neutral N-donor or one thiolate and four anionic O-donor ligands (5.30). Since a neutral N-donor and a hydride have very similar hardness parameters (6.9 vs 6.8), a hydride can be substituted for an N-donor with a similar result.

Comparison of the edge data obtained for *T. roseoperisicina* hydrogenase form C with the edge data published for reduced *D. gigas* hydrogenase[17] indicates that the latter enzyme has more S-donor ligands. The breadth of the edge and maximum normalized absorbance in the edge region (1.0) are clearly indicative of a ligand environment that is composed largely of S-donor ligands. This result is in agreement with the analysis of the EXAFS spectrum of the Ni center in this enzyme. The edge obtained for *T. roseopersicina* bears more resemblance to the edge obtained for the as isolated form of the enzyme from *Desulfovibrio baculatus*, an Fe,Ni,Se hydrogenase, where EXAFS analysis reveals evidence of S-, Se-, and O,N-donor ligands.[12] This edge also features the change in slope at low energy that is a feature of distorted trigonal-bipyramidal complexes and might arise from the presence of a 1s → $4p_z$ transition that could become apparent with a distortion toward pyramidal geometry.

(86) Crabtree, R. H. *Inorg. Chim. Acta* **1986**, *125*, L7.

Conclusion

The ability to use the XANES region for structural predictions in Ni complexes with mixed-ligand donor atoms has been examined and extends the information available from the analysis of EXAFS. EXAFS contains no information regarding geometry about the absorbing atom, and the number of scattering atoms is poorly determined. The XANES data accumulated from the Ni complexes examined in this work show that the predictions of coordination number/geometry based on the edge structure analyses of Scott et al. are useful, even in cases of low symmetry. However, these features become difficult to distinguish in complexes with large numbers of S-donor ligands (i.e. low edge energy). The area under the 1s → 3d transition is particularly useful in narrowing the possibilities of coordination number/geometry, since it appears to be relatively insensitive to mixed-ligand environments and distortions from ideal geometry. In addition, correlations between edge energy, edge slope, or the maximum absorbance of the edge region of the spectra and the average hardness of the ligand environment are useful in determining the number of hard vs soft donor atoms present. This provides a useful check of information concerning the nature of the ligand environment obtained from EXAFS analysis.

A comparison of the XANES regions of isoleptic Ni(II/III) pairs reveals that, in general, the Ni(III) features are broader and less distinct. Nonetheless, the same features still serve as useful indicators of changes in geometry. Edge energy shifts obtained for the same pairs of complexes reveal only small shifts to higher energy occur upon oxidation. These shifts are much smaller than those observed for changes in the ligand environment of Ni(II) complexes. Thus, without specific information regarding the nature of the ligand environment, edge energy cannot be used to determine formal oxidation state and edge energy shifts are not particularly useful indications of changes in formal oxidation state of the metal center.

XPS spectra were used to examine the binding energy of electrons on the Ni center and the donor atoms. These data reveal a trend toward increasing ligand oxidation in complexes with S-donor atoms. These data are in agreement with the small or nonexistent edge energy shifts that occur upon oxidation of Ni(II) complexes with S-donor ligands, including the Ni site in hydrogenase in all but the most reduced form, and suggest a substantial role for the S-donor ligands in the redox chemistry of the Ni site in hydrogenases.

On the basis of the results of this model study, an analysis of the Ni K-edge XANES spectrum obtained from a sample of *T. roseopersicina* hydrogenase is consistent with a distorted trigonal-bipyramidal geometry composed of a mixture of O,N- and S-donor ligands for this biological Ni site.

Acknowledgment. This work was supported by NIH Grant GM-38829 (M.J.M.). S.L.S. and W.S.W. wish to acknowledge support of the NSF under Grant CBT-8814974. P.K.M. thanks the donors of the Petroleum Research Fund, administered by the American Chemical Society, for support. We are grateful to Prof. Robert Scott for many insightful discussions and for data on *Desulfovibrio* hydrogenases used in making comparisons. We also wish to thank Prof. Larry Que, Dr. Anne True, Dr. Syed Khalid, and the staff at CHESS for experimental support. The technical assistance of Joyce P. Whitehead and Denise L. Driscoll in the purification of the enzyme is also acknowledged. We thank Prof. Robert M. Buchanan for the gift of compound **4**.